

Undrained creep failure of a drainage canal slope stabilized with deep cement mixing columns

Abstract This paper presents an analysis of the slope failure of a Suvarnabhumi drainage canal during construction. The Suvarnabhumi drainage canal project includes a large drainage canal with a road on both sides. The width of the bottom of the drainage canal is 48.0 m, the depth of the drainage canal is 3.0 m, and the length of the drainage canal is 10.5 km. Because the project was constructed on very soft Bangkok clay, deep cement mixing (DCM) columns were employed to increase the stability of the excavated canal. The failure of the drainage canal slope occurred 25 days after the end of excavation. The field monitoring data show that lateral movement of the canal slope continuously increased with time, which caused failure due to the instability of the canal slope. The time-dependent deformation and undrained creep behavior of very soft clay was suspected to be the cause of the canal failure. A laboratory investigation of undrained creep behavior and a finite element analysis (FEA) using the soft soil creep (SSC) model were performed to confirm the causes of the canal failure. The results indicate that very soft clay specimens that are subjected to deviator creep stress levels of 70 and 100 % of the peak strength failed by creep rupture within 60 days and 8 min, respectively. The factor of safety for the canal slope, which was obtained from the FEA, shows significant reduction from the initial value of 1.710 to 1.045 within 24 days after the end of excavation due to the effect of undrained creep. This paper also describes a solution method that is applied to a new section of the canal. Field monitoring and an FEA of the new trial section were performed to prove the effectiveness of the solution method.

Keywords Deep mixing · Failure · Finite element · Slope stability · Undrained creep

Introduction

Landslides are one of the most significant geologic hazards (Wang and Zhang 2014). Infrastructure projects, such as dams, drainage canals, roads, slope excavations, and slope protections, are generally subjected to slope failure. The required geological conditions at a construction site generally comprise shear strength and deformation behaviors, hydrogeological conditions, and geologic formation. Bangkok clay deposit is considered to be a problematic soft clay with a high deformation potential and a low shear strength (Lorenzo and Bergado 2004; Horpibulsuk et al. 2007). Slopes excavated in these soft clays exhibit viscous creep behaviors, in which deformation and movement proceed under a state of constant stress. Significant creep stress ultimately causes failure (Redman and Poulos 1984; Kuhn and Mitchell 1993). Undrained creep behavior can be divided into volumetric creep and deviator (or shear) creep according to the acting stress. Volumetric creep is caused by constant volumetric stress, whereas deviator creep is caused by constant deviator stress. Laboratory undrained creep tests of soil samples are usually performed on cylindrical specimens using an isotropically consolidated undrained (ICU) triaxial compression apparatus in a laboratory. Typical undrained creep

curves for a constant deviator stress that expresses axial creep strain (ε_{ac}) as a function of elapsed time (t) are shown in Fig. 1. According to the shape of the $\varepsilon_{ac}-t$ response curve, creep can be divided into primary, secondary, and tertiary phases (Arulanandan et al. 1971).

The primary phase can be defined as creep deformation during which the strain rate continuously decreases with time. Deformation at a constant rate (material flow) is denoted as the secondary phase. In the case of the tertiary or the accelerated phase, the strain rate is continuously increasing, which causes creep rupture. Generally, volumetric creep consists of the primary phase of creep deformation and tends to stabilize. As shown in Fig. 1, the shape of the $\varepsilon_{ac}-t$ response curve is primarily dependent on the relative magnitude of the applied deviator stress compared with the undrained strength (obtained from the ICU test) of the material at the same consolidation pressure. When the applied deviator stress is small compared with the undrained strength, the creep strain rate monotonically decreases with time. Curve A in Fig. 1 shows a typical $\varepsilon_{ac}-t$ response for this stress condition. For a relatively high deviator stress, the creep strain rate increases with time, which causes rupture of the sample. Curve C in Fig. 1 shows a typical curve for this response. An intermediate value of the deviator stress (compared with the undrained strength) may yield a response, as indicated by curve B in Fig. 1 (Faruque 1986). Saturated sensitive soft clay is most susceptible to this behavior.

During construction, the excavated slopes show deviator creep behavior accompanied by little or no dissipation of pore pressure at a constant shear stress due to the low permeability of soft clay. This continuing undrained creep may frequently cause failure of the slope, which implies that the undrained shear strength can be significantly reduced with time, as investigated through undrained triaxial creep tests by various researchers (Casagrande and Wilson 1951; Walker 1969; Holzer et al. 1973; Yin et al. 2002; Desai et al. 2011; Taechakumthorn and Rowe 2012). Therefore, analysis of the undrained creep behavior is important for estimating the long-term stability of a man-made slope. The continuous increase in shear deformation with a constant deviator creep stress (Fig. 1) induces an increase in excess pore water pressure (Δu) with time because the specimen is sheared for the condition of zero volume change (undrained). This creep process reflects the diminution of effective stress and an increase in the stress ratio q/p' (deviator stress to mean effective stress) toward the Mohr–Coulomb failure line (Wang and Yin 2014). An illustration of this process with the effective stress paths is provided in Fig. 2a, b. Thus, undrained creep behavior contradicts consolidation theory, which states that excess pore water pressure decreases with time due to drainage, which causes an increase in effective stress. An increase in creep time causes larger excess pore pressure at failure due to creep deformation (Campanella and Vaid 1974; Mitchell and Soga 2005; Leoni et al. 2008). Based on these facts, deviator creep in undrained conditions is extremely important in the analysis of stability problems. Chang et al. (2015) observed and simulated the

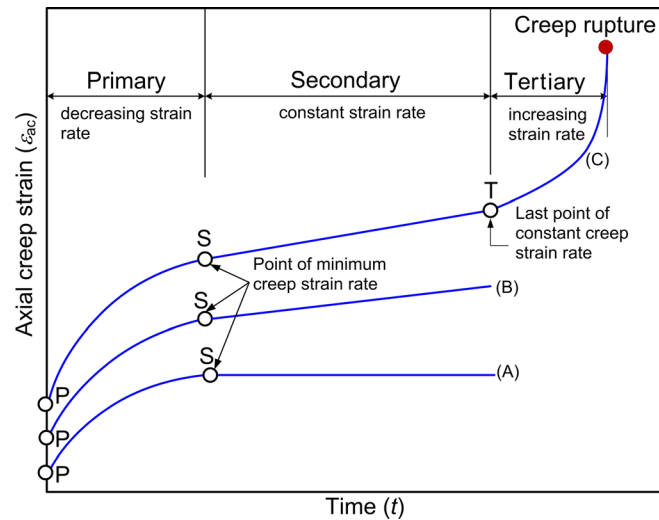


Fig. 1 Typical axial creep strain–time response curves for ICU triaxial compression test (Faruque 1986)

creep behavior of rock slope. The results of their study indicate that topography influences slope creep behavior. Slopes with significant inclination or height produce significant creep behavior.

A stabilizing pile and stone column can be employed to support these unstable slopes (Rogers and Glendinning 1997; Anbarasu et al. 2010; Kourkoulis et al. 2011; Vekli et al. 2012; Wang and Zhang 2014; Yu et al. 2015). The deep cement mixing (DCM) method is a ground improvement technique that has also been introduced to solve these problems. The DCM method has been employed in Japan, the Nordic countries, Thailand, China, the USA, the UK, Germany, and Poland among other countries. Cement additive in either slurry or powder form is injected into the ground and mixed with the in situ soil by mixing blades or jet grouting, which forms a hard-stabilized soil column that is referred to as a *DCM column* (Horpibulsuk et al. 2011, 2012; Shen et al. 2013a, b). The applications of DCM include foundation supports, slope protection, retention systems, ground treatments, liquefaction mitigation, hydraulic cutoff walls, and environmental remediation (DJM (Deep Jet Mixing) Research Group 1984). DCM column rows have been employed to increase the stability of slopes against horizontal or sliding forces (Broms 1999). Larsson et al. (2012) suggested the use of overlapping column rows for a better interaction with the surrounding soft soil and investigated the effect of the overlapping zone and the strength in this zone. However, failures have occurred, as demonstrated in a case study of slope failure in a large drainage canal project constructed in soft clay that is stabilized with DCM columns.

This paper investigates the failure of a drainage canal that is part of an excavation project in soft clay that is stabilized with DCM columns. It describes both the stabilizing methods for a new section of the canal and the subsequent evaluations that are conducted to prove their effectiveness. The “Description of a drainage canal project” section contains a general description of the drainage canal project. The “Field investigation” section describes the field monitoring results after the end of excavation and the failure investigations that are performed to assign the failure causes. The “Laboratory investigation” section presents a laboratory investigation of the creep behaviors of soft clay specimens that are collected from the field. The “Finite element analysis of

the field case study” section contains a detailed finite element analysis (FEA) of the drainage canal. The “Results of finite element

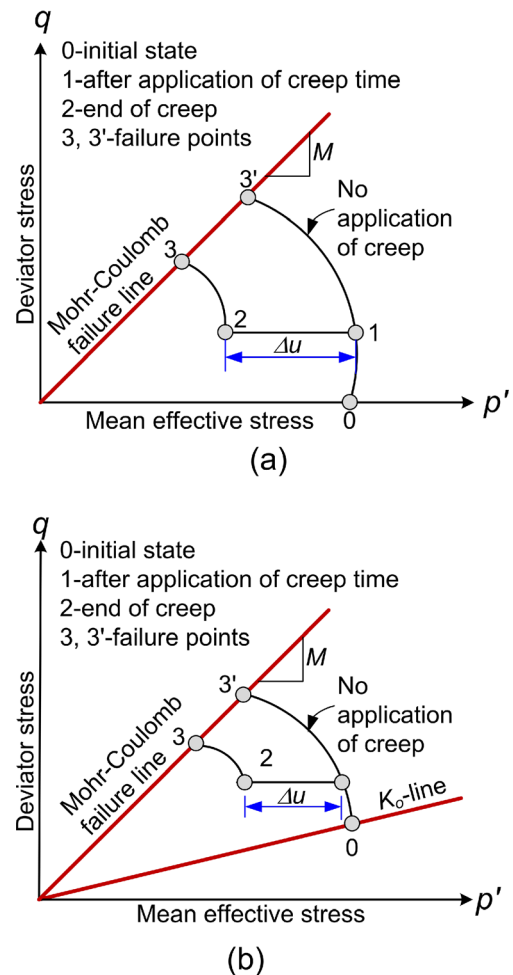


Fig. 2 The effect of undrained creep on the strength of normally consolidated clay in a ICU and b K_0 CU triaxial compression test (Mitchell and Soga 2005; Campanella and Vaid 1974)

analysis” section presents the results of the FEA of the drainage canal. The “Remedial measures” section describes the stabilizing method, the field monitoring results, and the FEA results to prove the effectiveness of the stabilizing method. The main conclusions are given in the “Conclusions” section.

Description of a drainage canal project

The field case study comprises the Suvarnabhumi drainage canal project, which is under the jurisdiction of the Royal Irrigation Department of Thailand, which is located in the Samut Prakan Province of Thailand. The main purpose of this project is to drain floodwater from the eastern region of Bangkok and the vicinity of the Suvarnabhumi International Airport. The project consisted of the excavation of a new canal, the construction of pumping stations, and the installation of a telemetry system. The width of the bottom of the drainage canal is 48.0 m, the depth of the drainage canal is 3.0 m, and the length of the drainage canal is 10.5 km. Two-lane roadways with a width of 11.0 m and a height of 2.4 m were constructed on both sides of the canal for transportation.

Figure 3 shows the soil profile and soil properties at the field case history site. The soil profile consisted of three layers: 10 m of very soft normally consolidated clay, 5 m of soft normally consolidated clay, and 3.5 m of medium stiff clay and 2.5 m of stiff clay. The natural water (w_n) content was near the liquid limit (LL), high water content was noted in the depth range of 2 to 10 m (>100 %), and lower water content was noted in the deeper layer. The undrained shear strength, which was measured using the field vane shear test, tended to increase with depth. DCM columns were applied to improve the soft clay layer.

It is well known that *soft Bangkok clay* has low shear strength and high w_n (high initial void ratio, e_o). The very soft clay is formed by deposition of marine clay on the Chao Phraya delta of Thailand. It is normally consolidated to lightly overconsolidated, with the overconsolidation ratio (OCR) varying from 1.0 to 1.5 (Bergado et al. 1996; Shibuya et al. 2003; Horpibulsuk et al. 2007). The degree of sensitivity of clay is defined as the ratio of the undrained shear strength in an undisturbed state to that in a remolded state. Any clay with the sensitivity ratio equal to or greater than 8 is classified as a quick clay based on classification of sensitive clays by Rosenqvist (1953). The calculated sensitivity ratios from the field vane shear test results ranged from 2.7 to 5.0. Thus, very soft clay in this project is not a quick clay although its natural water content was higher than LL. The strain-hardening behavior of very soft clay was observed under ICU triaxial compression test (Fig. 13a), which is a general behavior of normally consolidated clay.

A trial test section of the drainage canal was constructed prior to commencement of the project. The configuration of the DCM columns is shown in Fig. 4. The diameters of the DCM columns under the roadway (referred to as the bearing DCM columns) were 0.6 m; they were installed in a rectangular pattern with spacing of 1.50×1.75 m. Seven DCM columns (referred to as the DCM column rows) were installed in a row pattern at the canal slope with a spacing of 1.50 m. The additional DCM columns at the berm area were installed with spacing of 1.50×1.60 m to increase the slope stability. The required compressive strength of the DCM columns was 0.6 MPa. To attain the required compressive strength, 220 kg/m³ of cement was employed.

The DCM column rows located at the canal slope are designed to resist lateral force by their flexural resistance. Due to the low flexural resistance of a single DCM column, DCM column rows were employed. Unconfined compression tests were conducted to compare the obtained strength with the required strength. The unconfined compressive tests were completed on DCM column specimens, which were collected with a sampler at various depths. The collected specimens were cured for 30 days prior to testing. The variations in the unconfined compressive strength value (q_u) and the elastic modulus at 50 % of the unconfined compressive strength (E_u) of the DCM columns with depth are shown in Fig. 3; these values were obtained from the field specimens. The q_u ranged from 0.89 to 2.7 MPa, which exceeds the required strength (0.6 MPa). Therefore, the low quality of the DCM columns may not be the cause of failure of this canal project. The dashed lines of the q_u and E_u profiles in Fig. 3 represent the average values in the numerical analysis.

The construction plan was divided into four stages: first, the DCM columns were installed; second, the 1.2-m-high berm was constructed using silty sand fill material; third, the canal was excavated to a depth of 3.0 m; and last, the roadway was constructed to a height of 2.4 m. Three inclinometers were installed after the excavation of 1.5 m to monitor lateral movements during excavation of the remaining 1.5 m.

Field investigation

Figure 5 displays the profiles of lateral movement with depth after the end of excavation at a depth of 3.00 m, which were obtained from inclinometers at three locations: I-1, I-2, and I-3. The field data revealed that the maximum lateral movement immediately after the end of excavation was 10 mm. As the roadway attained its final elevation of 2.40 m after 14 days, the maximum lateral movement increased to 40 mm at inclinometer I-1. The lateral movement at all locations continuously increased with time until eventual failure at 25 days, as shown in Fig. 6. The failure extended throughout the berm area, while the base of the canal heaved. The DCM column rows also tilted toward the canal. Based on the field observations, the first crack of the slope instability occurred at the berm area above the additional DCM columns and the potential slip surfaces revealed that the translation of soil mass dominated to a depth of 7.5 m. The lateral movement obtained from inclinometer I-1 indicates that the development of a shear zone occurs at the depth range of 5.0 to 9.0 m. The increasing lateral movement with time is caused by the process of undrained creep at constant deviator stress. Figure 7 displays the plot of the maximum lateral movements with elapsed time at the end of excavation. The curve of the lateral movement against time of the very soft clay located near the excavation base, which was obtained from inclinometer I-1 (Fig. 7a), is similar to $\varepsilon_{ac}-t$ response curve C of the deviator creep behavior, as shown in Fig. 1.

The rate of lateral movement in the secondary stage is constant prior to the tertiary stages and failure conditions, according to the surface rupture observed in the field. The level of deviator stress induced by the slope excavation is sufficient for the development of the shear mobilization of all three phases due to a lack of soil stabilization by the DCM columns. The average increase in the rate of lateral movement in this study was defined as the difference in lateral movement divided by the elapsed time. Thus, the average rate of lateral movement for the case history after the end of

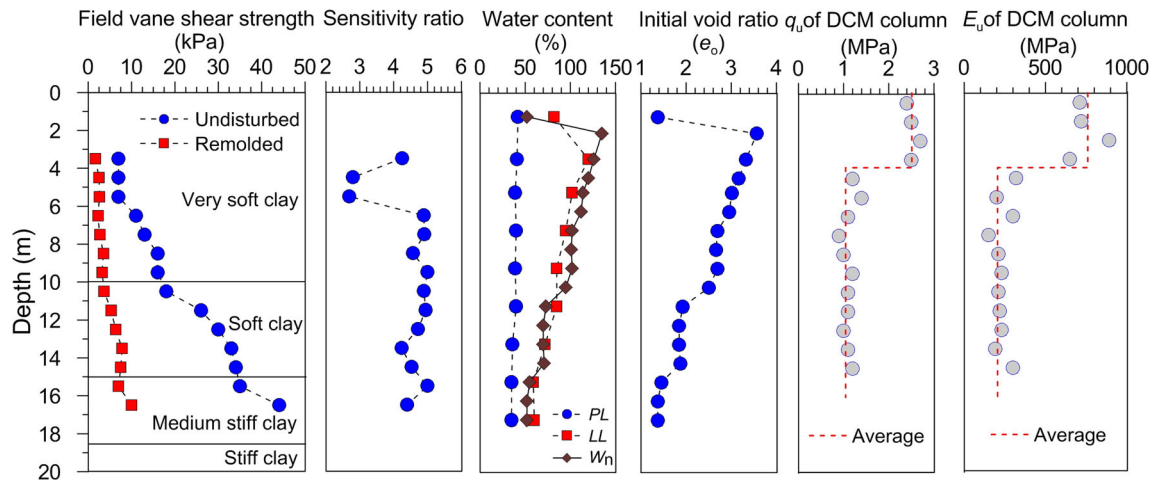


Fig. 3 Soil and DCM column properties

excavation (0 day) to 25 days (canal failure) was $(60-10)/(25-0)=2$ mm/day for I-1. Figure 7b shows that the rate of lateral movement of the soft clay located in the berm area with DCM column rows (I-2) was constant at 15 days after the end of excavation and was considered to be the secondary phase. The tertiary stage (accelerated phase) was not distinct, which indicates that the creep behavior of this location is similar to curve B in Fig. 1, which implies that the soft clay located at I-2 was subjected to a moderate deviator creep level. However, the soft clay slope in this location failed due to the inability of the DCM column rows to stabilize the creep failure. Therefore, the deformation–time response in curve B (Fig. 1) is responsible for the slope failure in the field condition. However, the lateral movements from inclinometer I-3 show distinctly different creep behaviors compared with the data from inclinometers I-1 and I-2. The soft clay under the roadways, which improved with individual DCM columns (I-3), was also subjected to primary creep for 18 days prior to the constant rate of lateral movement in the secondary stage (Fig. 7c). The creep deformation tended to stabilize after 18 days without a tertiary stage, which corresponds to $\varepsilon_{ac}-t$ response curve A in Fig. 1. No slope failure of the drainage canal located in I-3 was observed because creep deformation cannot develop to the rupture stage, which is consistent with the creep behavior exhibited by curve A in Fig. 1.

Laboratory investigation

Test program

Based on the field observation of the case history, the failure mechanism of the Suvarnabhumi drainage canal was undrained creep failure because the excavated canal slope experienced no surcharge for 25 days. Thus, the undrained creep behavior of soft Bangkok clay required verification. After the canal slope failed, laboratory investigations were performed. Soft clay specimens were collected near the trial section at the depth range of 3.0–4.0 m. The testing program consisted of consolidated undrained triaxial compression tests, including ICU tests, ICU creep tests, and K_0 consolidated undrained (K_0 CU) creep tests. The objectives of the ICU tests determined the undrained shear strength and shear strength parameters, whereas the ICU and K_0 CU creep tests determined the undrained creep characteristics, respectively. The

ICU tests were conducted according to ASTM (2012). The following isotropically consolidated pressures (p_o') were employed in this study: 20, 50, 80, and 100 kPa. The effective stress paths ($p'-q$) for the ICU tests are plotted in Fig. 8. The relationship between the slope of the Mohr–Coulomb failure line (M) and the friction angle (ϕ') can be expressed by the following equation:

$$M = \frac{6 \sin \phi'}{3 - \sin \phi'} \quad (1)$$

Thus, the parameter M for the very soft clay in this study was 1.07, which corresponds to a friction angle (ϕ') of 27° . The ICU test with a p_o' value of 50 kPa was selected to specify the peak deviator stress for the calculation of the stress levels because this confining pressure was similar to the effective overburden pressure at the middle of the thickness of the soft clay. The peak deviator stress (q_{peak}) for the ICU test with a p_o' value of 50 kPa was 40 kPa.

The axial loads for the undrained creep tests were applied in single increments with a p_o' value of 50 kPa, and the axial deformation versus time was recorded. Three different deviator creep stress levels with the stress ratio (q/q_{peak}) of 50, 70, and 90 % (refer to Table 1), which corresponds to a factor of safety of 2.0, 1.43, and 1.11, respectively, were applied to perform the ICU creep tests. Natural soft clay is usually deposited in a K_0 -consolidated condition. Additional loads are usually added during construction, which causes the creeping of soil. Thus, a series of undrained creep tests on K_0 -consolidated clay samples were also performed with a mean effective stress of $p_o'=50$ kPa and a deviator stress of $q_o=32.6$ kPa with a duration of 2 days prior to shearing. Three different deviator creep stress levels with $q/q_{peak}=85$, 95, and 100% (refer to Table 1) correspond to a factor of safety of 1.18, 1.05, and 1.00, respectively. The numerical values of the creep stresses for all the tests in this study are tabulated in Table 1.

Undrained creep test results

Figures 9 and 10 show the similar trend in the development of axial strain with time for various creep stress levels in the ICU and K_0 CU tests. The specimen that was subjected to a creep stress level

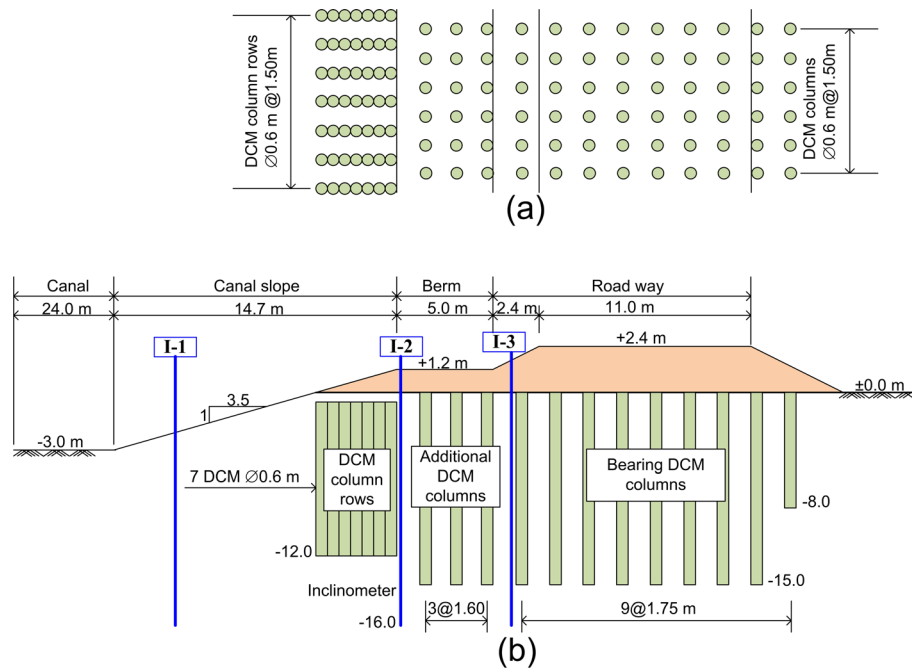


Fig. 4 Configuration of drainage canal stabilized with DCM columns: a plan view and b section view

of 50 % (Fig. 9a) shows a small increase in strain after initial deformation. No failure was observed within the testing time due to the low deviator stress level, which corresponds to the field observation of soft clay at I-3. However, the specimens at creep stress levels of 70 and 90 %, as shown in Fig. 9b, c, respectively, were progressively strained with time until eventual failure. The tertiary stage began 60 and 25 days for the specimens at creep stress levels of 70 and 90 %, respectively. Figure 10a–c shows that a similar creep behavior of the specimens in the K_0 CU tests with the tertiary stage was observed after 25 days, 3.5 days, and 6 min for the specimens at creep stress levels of 85, 95, and 100 %, respectively. The creep strains and time to rupture were higher and faster, respectively, for the specimens with higher creep stress

levels. Therefore, the deviator stress level accelerates the time to failure by creep rupture. The soft clay located at I-1 behaved in a similar manner to these specimens. Thus, this laboratory test confirmed that the soft clay located at I-1 was subjected to a high deviator creep level, which produced a lower factor of safety than the factor of safety obtained for other locations that improved with DCM columns. Lateral movement–time curves I-1 and I-2 are similar to the $\varepsilon_{ac}-t$ response curves of K_0 CU tests compared with the lateral movement–time curves of the ICU tests, which implies that the field undrained creep behavior is consistent with the K_0 CU creep behavior in the laboratory. This finding is consistent with the undrained creep test results of Campanella and Vaid (1974), who concluded that some differences in the deformation–

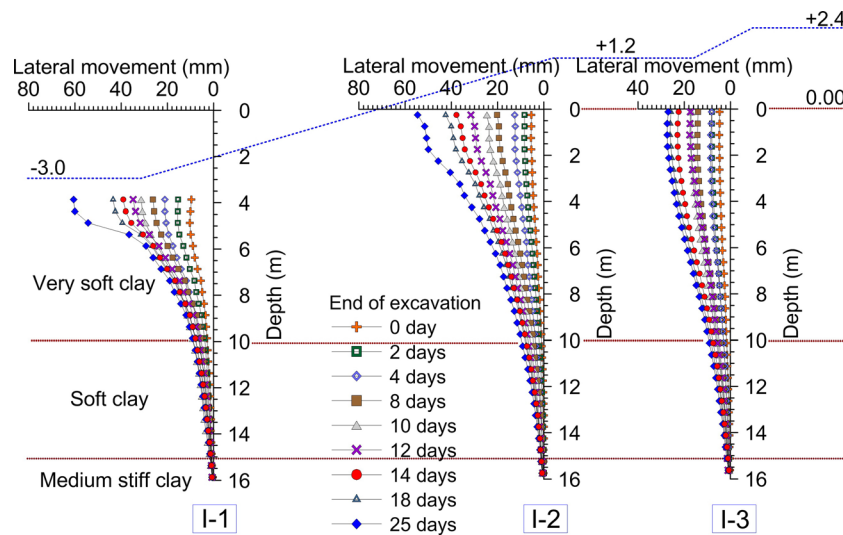


Fig. 5 Lateral movement profiles

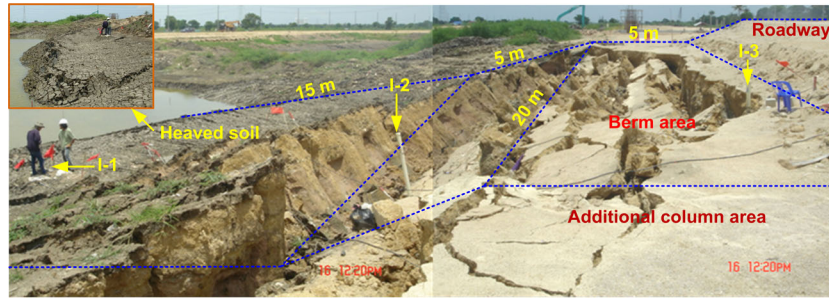


Fig. 6 Failure of field trial test

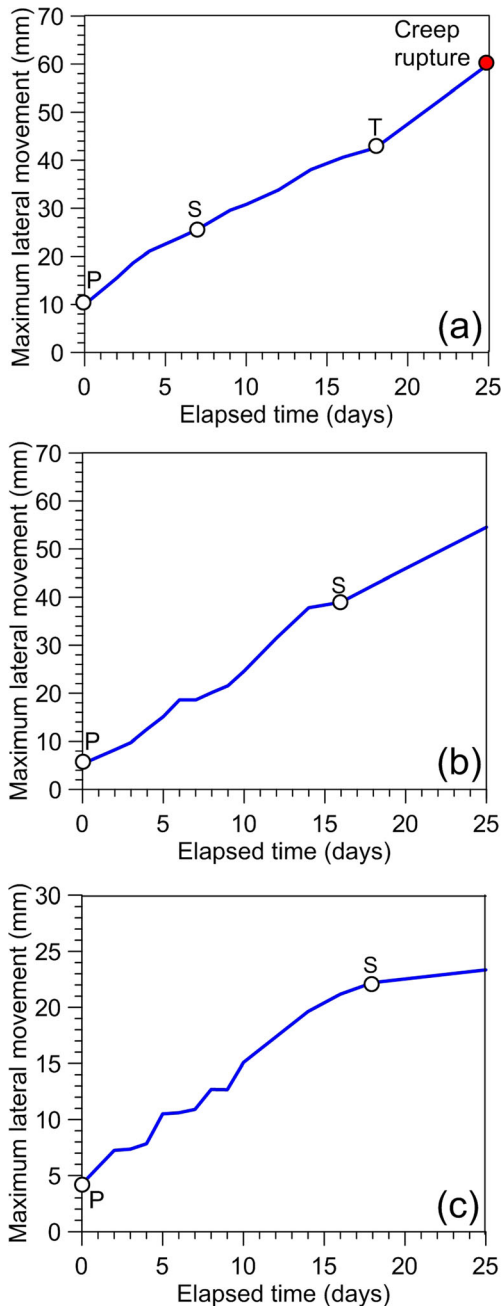


Fig. 7 Maximum lateral movements of soft clay at the end of excavation at three locations: a) I-1, b) I-2, and c) I-3

time curves between the ICU and K_0 CU tests may occur because soft clay deposits in nature have been subjected to an anisotropic stress history and deformation conditions conform to the K_0 condition compared with isotropic compression.

Finite element analysis of the field case study

Finite element mesh and boundary condition

A finite element simulation was performed to explain the failure mechanism of the canal slope by undrained creep using the PLAXIS 3D software, version 2013. The 3D finite element model consisted of the DCM columns, the embankment, and the foundation soils. The soil volume is modeled by ten-node tetrahedral volume elements. The ten-node tetrahedral volume elements are created in the 3D mesh procedure. This type of element provides a second-order interpolation of displacements.

Note that the large deformation is necessarily considered for problems of dynamic evolution of slides in unstable slopes. However, this study focuses on the causes of the canal failure, not the simulation on the progressive failure analysis in which the traditional finite element method (FEM) is limited. It is believed that the deformations captured in this study (observed lateral movement) during the construction are still in the normal strain range in which the traditional FEM is applicable. To capture the evolution of slides in unstable slopes, sophisticated numerical methods, taking into account the large deformation (such as total

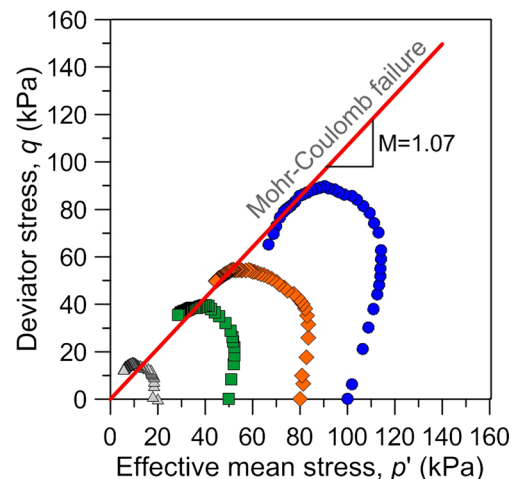


Fig. 8 Effective stress paths from ICU tests of very soft clay specimens

Table 1 List of undrained triaxial creep tests of very soft Bangkok clay

Test	Initial condition of test specimen	Creep stress level (%)	Increment deviator creep stress form initial condition, Δq (kPa)	Deviator creep stress, q (kPa)
ICU creep 1	Isotropically consolidated at $p_o = 50$ kPa	50	20	20
ICU creep 2		70	28	28
ICU creep 3		90	36	36
K_o CU creep 1	K_o consolidated at $p'_o = 50$ kPa, $q_o = 32.6$ kPa	85	1.4	34
K_o CU creep 2		95	5.4	38
K_o CU creep 3		100	7.4	40

Lagrangian and the update Lagrangian finite element as comprehensively reviewed by Wang et al. (2015), are necessary.

The configuration of the drainage canal, which is shown in Fig. 4a, is 3D because each DCM column is not continuous in the out-of-plane direction. Thus, it can be modeled as a 3D slice by planes of symmetry. Figure 11 illustrates the 3D finite element mesh, which consists of 11,380 elements and 17,544 nodes, that corresponds to the drainage canal configuration in Fig. 4a, b. At the bottom of the finite element mesh, the displacements are set to zero in three directions: x , y , and z . The vertical model boundaries parallel to the yz plane are fixed in the x direction and are free in the y and z directions. In addition, the symmetrical conditions imply that vertical model boundaries parallel to the xz plane are fixed in the y direction and are free in the x and z directions. The length and the depth of the model were 80 and 30 m, respectively, to prevent boundary effects, and the width of the model was 1.5 m due to a symmetrical condition. The circular columns were modeled as octagonal cylindrical sections with the same cross-sectional area as circular columns with a diameter of 0.6 m. The construction stages of the finite element calculation are as follows:

- Stage 0 generation of the initial stresses in the K_o condition
- Stage 1 installation of DCM columns and construction of 1.2-m-high berm
- Stage 2 excavation of -1.50 m
- Stage 3 excavation of -3.0 m and starting the measurement of lateral movement at the locations of I-1, I-2, and I-3
- Stage 4 construction of a 2.4-m-high roadway

Constitutive model and model parameters

The Mohr–Coulomb (MC) model is a simple elastic-perfectly plastic model. The DCM columns and the roadway were modeled as the MC model (Huang and Han 2009; Mun et al. 2012; Voottipruex et al. 2011a, b; Jamsawang et al. 2015). The tensile strength of the DCM columns, which were considered using the tension cutoff in the model, was 16 % of q_u (Jamsawang et al. 2010). The linear elastic-perfectly plastic Mohr–Coulomb model requires five

parameters, which are generally familiar to the majority of geotechnical engineers and can be obtained from basic tests on soil samples. These parameters and their standard units are as follows: Young’s modulus (E), Poisson’s ratio (ν), cohesion (c), friction angle (ϕ), and dilatancy angle (ψ). Undrained type C was employed to simulate undrained behavior of the DCM column using a total stress analysis with direct input of the undrained shear strength, i.e., setting the friction angle to zero and the cohesion to the undrained shear strength ($\phi=0$; $c=c_u$). In this study, the undrained shear strength of the DCM column is half the unconfined compressive strength of the DCM column (q_u). Stiffness is modeled using undrained Young’s modulus (E_u) and undrained Poisson’s ratio (ν_u). Undrained Poisson’s ratio of 0.495, which is almost 0.5, is selected. The parameters of the MC model are listed in Table 2.

The soft soil creep (SSC) model was applied to model the undrained creep behavior of the very soft clay and the soft clay. The SSC model is described by Vermeer and Neher (1999). It is an elasto-viscoplastic model with strain increments or strain rates divided into elastic and viscoplastic components. The SSC model has five main parameters. The modified compression index (λ^*) and the modified swelling index (κ^*) define the loading behavior and unloading volumetric behavior, respectively. The modified creep index (μ^*) defines the time-dependent creep behavior. The cohesion (c) and the friction angle (ϕ) define the strength of a material. A relationship among the internationally recognized parameters for the 1D compression index (C_c), the swelling index (C_s), and the initial void ratio (e_o) exists. These relationships are $\lambda^* = C_c/2.3(1+e_o)$ and $\kappa^* = 2C_s/2.3(1+e_o)$. In this study, a conventional odometer test of a very soft clay specimen that was taken from the project site at a depth of -4.0 was performed to obtain the parameters C_c and C_s . The test results are presented in the form of e - $\log\sigma'_1$ curves, as shown in Fig. 12. The values of C_c and C_s were 1.76 and 0.27, respectively. Thus, the corresponding values of λ^* and κ^* were 0.18 and 0.06, respectively, using $e_o=3.25$ in the calculations. Therefore, the suitable parameters of the very soft clay used for the FEA in this study are listed in Table 3. The parameters of soft clay were obtained from previous studies in

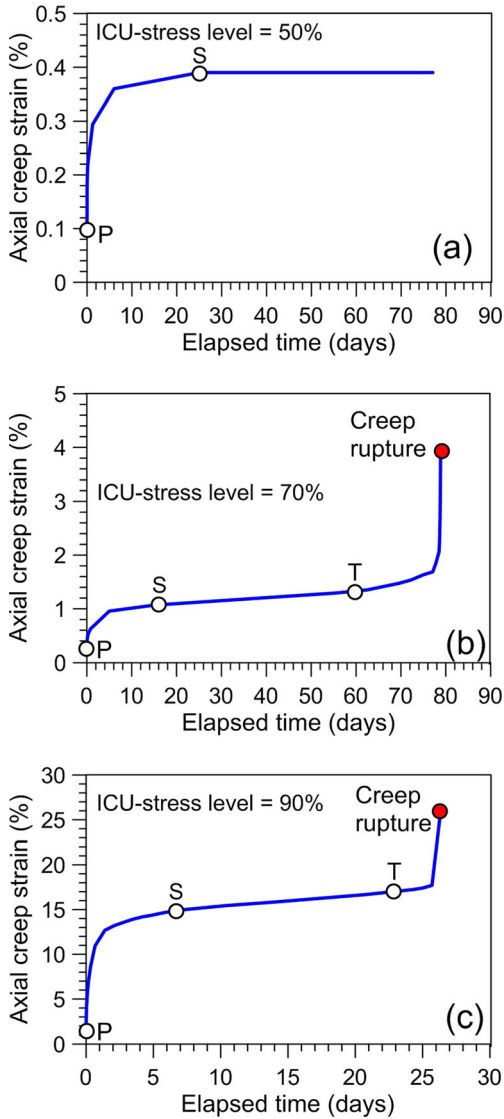


Fig. 9 Undrained creep behavior in ICU tests of very soft clay specimens at three creep stress levels: a 50 %, b 70 %, and c 90 % of peak strength

the vicinity of the canal project by Bergado et al. (2006) and Lin et al. (2006).

The hardening soil (HS) model is an advanced model for simulating the behavior of different types of soft soils and stiff soils (Surarak et al. 2012; Sexton and McCabe 2013; Jamsawang et al. 2015). The HS model utilizes four basic deformation parameters: the secant stiffness in standard drained triaxial tests (E_{50}^{ref}), the tangential stiffness for primary oedometer loading (E_{oed}^{ref}), the unloading and reloading stiffness (E_{ur}^{ref}), and the power of the stress level dependency of the stiffness (m) and shear strength parameters according to the MCM (c and ϕ). E_{50}^{ref} and E_{oed}^{ref} are set as the same value by defaults of the PLAXIS 3D software, version 2013. The tangential stiffness and secant stiffness are set as the same value by defaults of the PLAXIS 3D software, version 2013. The HS model was applied to model the behavior of the medium stiff clay and the stiff clay in this study using the Bangkok

subsoil parameters from Rukdeechai et al. (2009). The parameters in the HS model are listed in Table 4.

Calibration of SSC model

The PLAXIS “soil test” facility has been employed to simulate the undrained creep behavior of the very soft clay using SSC model. First, the ICU test results for a confining stress of 50 kPa were calibrated without the creep effect (no application of creep time) using the soil parameters in Fig. 12. The calibrated results are presented in Fig. 13a–c in terms of axial stress–axial strain, excess pore water pressure–axial strain, and p – q stress path relationships. The results of numerical simulation are in agreement with the test data, which implies that the calibrated soil parameters are reasonable. A parametric study of the influence of creep time on the ICU test results is also performed.

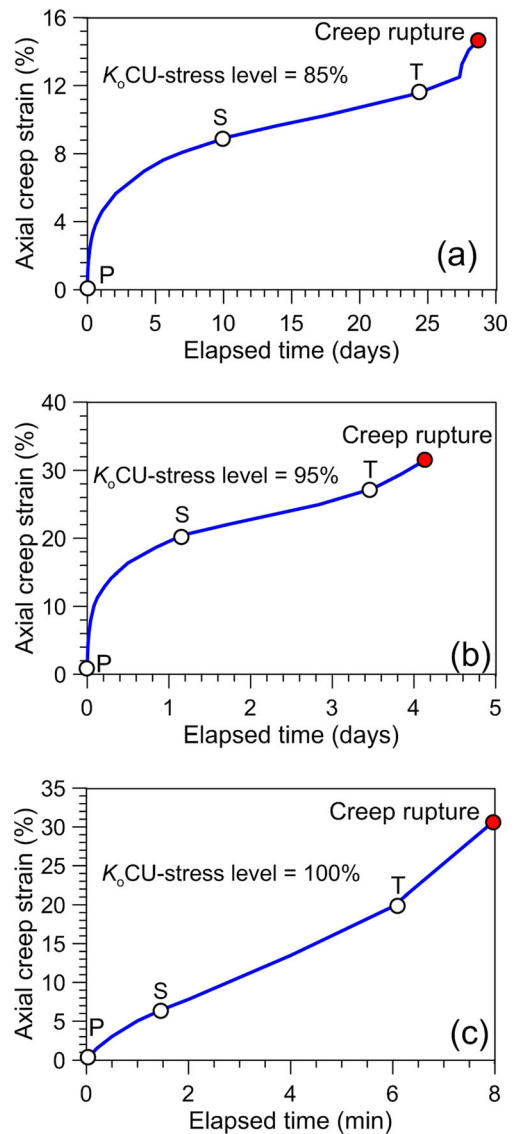


Fig. 10 Undrained creep behavior under ICU tests of very soft clay specimens at three creep stress levels: a 50 % b 70 %, and c 90 % of peak strength

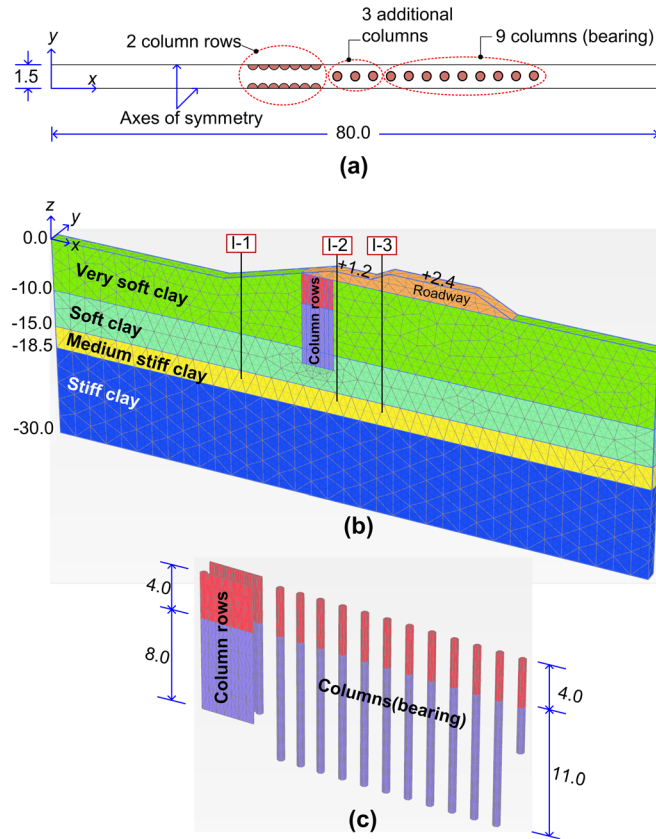


Fig. 11 a Plan view of the analysis zone, b 3D finite element mesh, and c enlargement of modeling column rows and columns in bearing zone

According to the results summarized by Mesri and Godlewski (1977), the values of μ^*/λ^* vary between 0.02 and 0.1 for different types of soils. The value of 0.088, which corresponds to the modified creep index (μ^*) of 0.016, which is a back-analyzed value for the field simulation in the “Results of finite element analysis” section, was selected to perform a parametric study. The creep time is simulated by applying prescribed displacements at different velocities. A total of 10 % axial strain is applied after 5, 15, 30, and 60 days. Figure 13a shows the influence of creep time on the stress–strain curves. The results show that both the stiffness and the peak deviator stress (strength) decreased with an increase in creep time. The reduced stiffness reflects that deformation

increases with time under a constant deviator stress. The shear strength and the stiffness are highly dependent on the creep time; the higher the creep time, the lower are the shear strength and the stiffness. At a given deviator stress, the generated pore pressure was larger for a slower creep time as a result of greater creep for a slow creep time, as shown in Fig. 13b. Figure 13c shows the corresponding p – q stress paths for Fig. 13a, b. For a slower creep time, a larger reduction in the mean effective stress due to the development of higher excess pore water pressure produces a smaller ultimate deviator stress. All the simulated results are consistent with the experimental data reported by Lefebvre and LeBouef (1987), Arulanandan et al. (1971), Leoni et al. (2008), and Wang

Table 2 Parameters of MC model

	DCM column	Roadway
Unit weight, γ (kN/m ³)	15	20
Elastic modulus, E (MPa)	750 for depth 0 to 4 m 200 for depth 4 to 15 m	7.5
Poisson’s ratio, ν	0.495	0.33
Cohesion, c (MPa)	1.25 for depth 0 to 4 m 0.5 for depth 4 to 15 m	0.01
Friction angle, ϕ (°)	0	30
Material behavior	Undrained	Drained

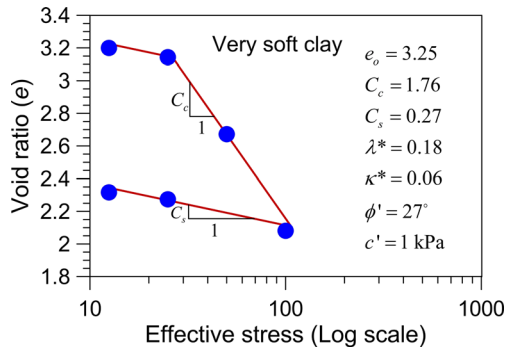


Fig. 12 Determination of soil parameters from odometer test results for a very soft clay

and Yin (2014). The SSC model appears suitable for modeling the undrained creep behavior of very soft clay.

Calculation of the factor of safety

A shear strength reduction or ϕ - c reduction method, which is an available option in the PLAXIS 3D software, version 2013, was used to compute the factor of safety of the slope. In the ϕ - c reduction approach, the strength parameters $\tan \phi$ and c of the soil are reduced until failure of the structure. The total multiplier ($\sum Msf$) defines the value of the soil strength parameters at a given stage in the analysis

$$\sum Msf = \frac{\tan \phi_{\text{input}}}{\tan \phi_{\text{reduced}}} = \frac{c_{\text{input}}}{c_{\text{reduced}}} \quad (2)$$

where the strength parameters $\tan \phi_{\text{input}}$ and c_{input} refer to the properties entered in the material sets and the strength parameters $\tan \phi_{\text{reduced}}$ and c_{reduced} refer to the reduced values in the analysis. $\sum Msf$ is set to 1.0 at the beginning of the calculation to set all material strengths to their unreduced values. The incremental Msf is employed to specify the increment of the strength of the first calculation step. The final step should yield a completely

developed failure mechanism. In this case, the factor of safety is as follows:

$$FS = \text{Value of } \sum Msf \text{ at failure} = \frac{\text{input strength}}{\text{reduced strength at failure}} \quad (3)$$

Results of finite element analysis

Verification of soil parameters

To verify that the parameters obtained from the laboratory test are suitable for simulating the field conditions, lateral movement profiles for the locations I-1, I-2, and I-3 immediately after the excavation stage were constructed with simulated data. At this stage, no creep time was applied. Thus, no creep effects from the SSC model were included in the simulated data. The results imply that the initial parameters of very soft clay obtained from the odometer test in Fig. 12 were overestimated due to the large strain effect that is frequently observed in conventional soil testing (Atkinson and Sallfors 1991). Unloading-reloading parameters are more sensitive to lateral deformation compared with loading parameters. Thus, only the reloading-unloading stiffness parameter κ^* was reduced from the initial input value of 0.06 to match the measured lateral movement profile to the simulated lateral movements. The back-calculated value for κ^* was 0.015, which yields the best fit of the lateral movement profile as shown in Fig. 14a-c (0 day after excavation), and fall within the range of κ^*/λ^* for very soft Bangkok clay reported by Bergado et al. (2006).

Back-analyzed modified creep index

Figure 14a-c shows the comparisons between the measured lateral movement profiles and the observed lateral movement profiles with time for the very soft clays at the three locations of I-1, I-2, and I-3 at the end of excavation, respectively. Due to the variations in the modified creep index μ^* in the field reported by Fatahi et al. (2013), the calibration of the field observation results and the SSC model was performed using 3D FEM models to obtain a

Table 3 Parameters of SSC model

	Very soft clay	Soft clay
Unit weight, γ (kN/m ³)	13.6	15.4
Modified compression index, λ^*	0.22	0.10
Modified swelling index, κ^*	0.015	0.02
Modified creep, μ^*	0.016	0.002
Poisson's ratio, ν	0.15	0.15
Cohesion, c (kPa)	1	2
Friction angle, ϕ (°)	27	27
Overconsolidation ratio (OCR)	1.2	1.5
Material behavior	Undrained	Undrained

Table 4 Parameters of HS model

	Medium stiff clay	Stiff clay
Unit weight, γ (kN/m ³)	16.5	19
Secant stiffness, E_{50}^{ref} (MPa)	20	60
Tangential stiffness, E_{oed}^{ref} (MPa)	20	60
Unloading and reloading stiffness, E_{ur}^{ref} (MPa)	60	180
Power of the stress level dependency of the stiffness, m	1	1
Poisson's ratio, ν	0.2	0.2
Cohesion, c (kPa)	10	18
Friction angle, ϕ (°)	27	27
Over consolidation ratio (OCR)	6	10
Material behavior	Undrained	Undrained

reasonable modified creep index to simulate the undrained creep behavior of the excavated slope in very soft clay. The value of μ^* for the very soft clay was varied to match the measured lateral movement profile to the calculated lateral movements and the elapsed time, in which the failure of the canal occurred (after 25 days). The higher values of μ^* cause larger lateral movement and faster slope failure due to the undrained creep effect. The back-calculated value for μ^* was 0.016, which yielded the best fit with the lateral movement profiles and caused the soil body collapse after 25 days, and fall within the range of the μ^*/λ^* value for soft organic clays proposed by Mesri and Godlewski (1977). Figure 15a shows the deformed mesh of the modeled canal with the back-calculated μ^* value of 0.016 and the elapsed time of 25 days. The berm area settled to the very soft clay layer. The very soft clay at the base of the canal heaved, and the DCM column rows tilted and moved toward the excavated canal, which was similar to the conditions shown in Fig. 6. The plastic points in the PLAXIS 3D software, version 2013, show the stress points that are in a plastic state (failure point); they are displayed in a plot of the undeformed geometry. The plastic point indicates that the stresses lie on the surface of the failure envelope. Figure 15b shows the distribution of the failure points in the 3D mesh, which is similar to the shape of the failure zone observed in the field (Fig. 6).

Stability analysis of the case history

Figure 16 shows the potential slip surfaces for the case history. The calculation results show that the initial factor of safety for the excavated slope with the 1.2-m-high roadway was 1.710. The values of the factors of safety exceeded the minimum required value of 1.30 during construction when undrained creep behavior was not considered. After the end of excavation, undrained creep was applied with a constant rate of creep strain until failure of the canal slope. Figure 17 shows the factor of safety versus time at the end of construction. The factor of safety decreases with an increase in time, as expected. The factor of safety decreases from the initial value of 1.710 to 1.30 at 8 days, which indicates that the factor of safety is less than the minimum required value after 8 days, which

demonstrates high potential for instability. The factor of safety decreases until the value of 1.045 is attained after 24 days; after 25 days, the FEA shows the soil body collapse that corresponds to the failure pattern shown in Fig. 7. The average rate of decrease of the factor of safety in this study was defined as the difference in the factor of safety divided the elapsed time. Thus, the average rate of the factor of safety decreases for the case history from the end of excavation (0 day) to 24 days was $(1.710-1.045)/(24-0)=0.0277/\text{day}$.

The behavior of the case history can be considered to be approximately undrained during the excavation period due to the very low permeability of the soft clay. The excess pore pressure increments are dependent on the path. The increase in the compression stress and the increase in the tension stress in the theoretical stress transfer in the undrained triaxial tests (Borges and Guerra 2014) are considered to be positive and negative, respectively. There was an increase in the theoretical stress in an undrained triaxial test with a compression stress path. In an extension stress path (as in an excavation zone), the direction of the pore pressure increments is opposite to the direction of the compression stress path. In an extension stress path, the increment of pore pressure Δu is negative (negative excess pore pressure). Because the total mean stress declines but the volume of soil does not change (undrained behavior), negative excess pore pressure is generated.

Figure 18(b) shows the results for excess pore pressure prior to excavation for the case history. Excess pore pressure is defined as the difference between the pore pressure at a particular instant and its initial hydrostatic value (Fig. 18(a)). Positive values of excess pore pressure are generated in the soft clay under the roadway due to the effect of embankment loading. Figure 18(c) shows that negative values are generated after the end of excavation on the excavation side. The highest negative value of excess pore pressure occurs below the excavation base due to the highest reduction of total mean stress in that zone. The undrained creep process begins after the end of excavation. Figure 18(d, e) shows the decrease in the negative pore water pressure at the end of excavation for 2 and 12 days, respectively, due to the effect of deviator creep. The value

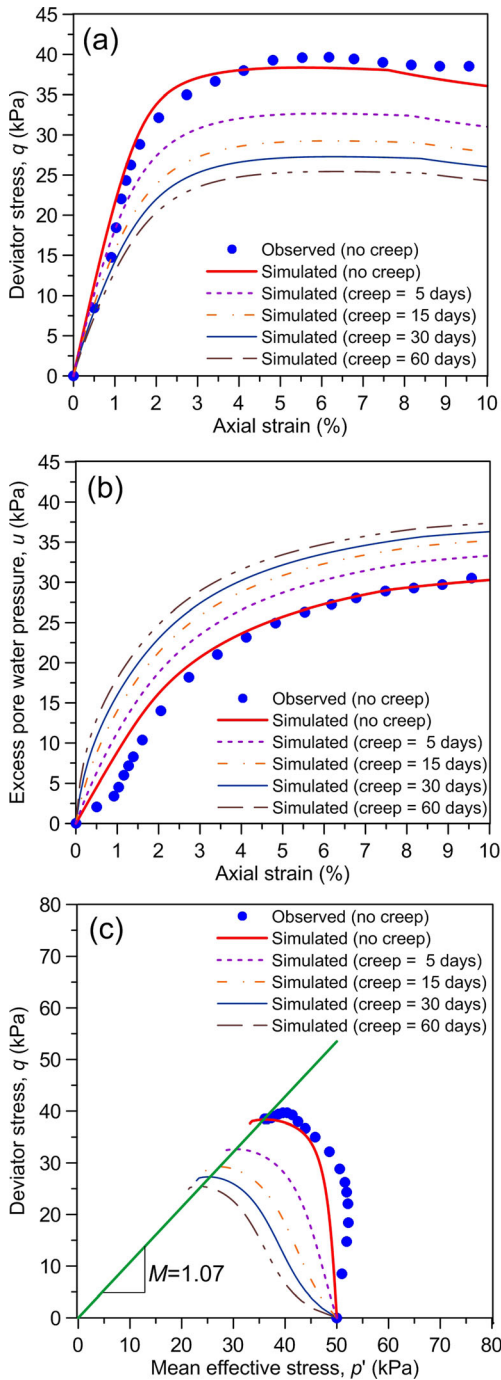


Fig. 13 Simulation of ICU test results and parametric study using the SSC model with calibrated parameters: a deviator–axial strain response, b excess pore water pressure–axial strain response, and c p' – q stress path

of the excess pore water pressure along the canal slope at failure approached positive values, as shown in Fig. 18(f). Undrained creep causes an increase in additional positive excess pore water pressure with time for constant deviator stress.

The mean effective stress decreases with time, which implies that the soft clay is subjected to the compression stress path and causes changes in its strength, as shown in Fig. 19. Figure 19 illustrates the stress path of point A in Fig. 18(b). The stress path began at the initial state of the soil (Fig. 18(a)) followed by

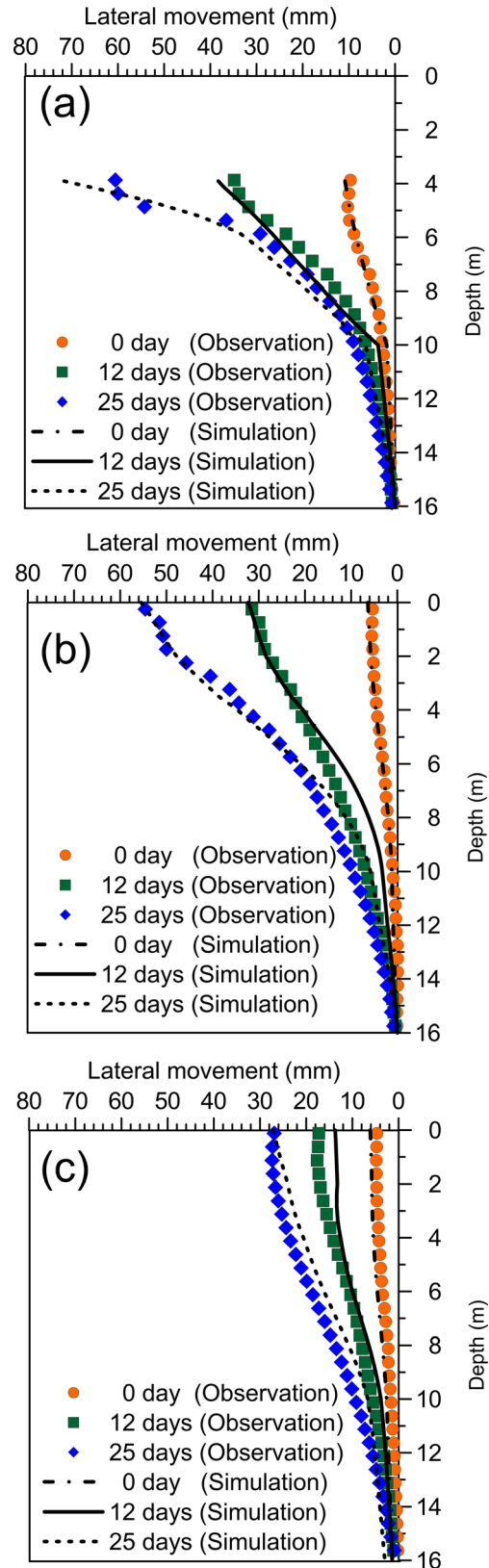


Fig. 14 Comparison between FEM results and field measurement data: a I-1, b I-2, and c I-3

the end of the excavation state (Fig. 18(c)). The undrained creep continued from stages 2 to 5. The stress path reached the Mohr–

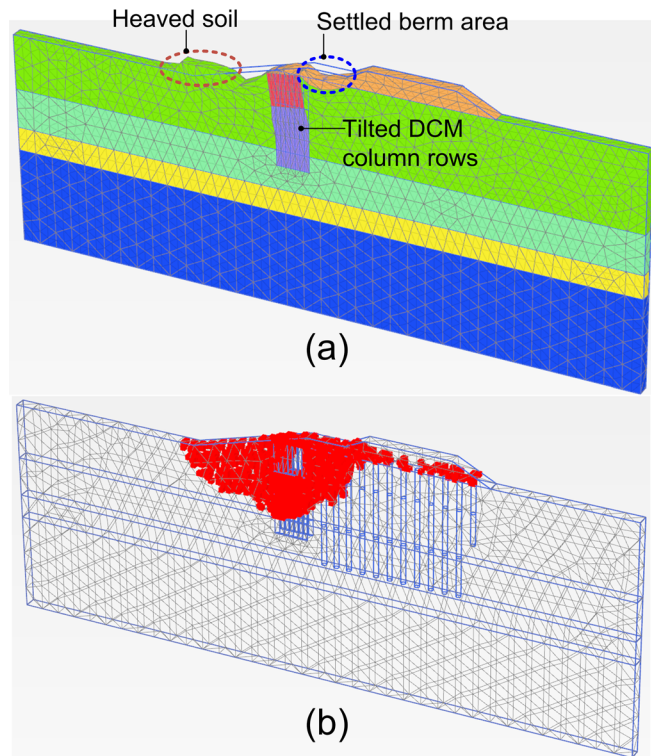


Fig. 15 a Deformed mesh and b distribution of plastic points of drainage canal in soil body collapse at 25 days

Coulomb failure line. The excess pore water pressure (Δu) developed during the undrained creep, which reduces the strength of soft clay similar to the behavior in Fig. 2b. This process causes the factor of safety, as shown in Fig. 16, to decrease with an increase in time. Thus, the results from the FEA confirm that the canal in the case history failed due to the undrained creep process.

Remedial measures

The results of the analysis in the previous section revealed that the cause of the canal slope failure was undrained creep failure caused by a delay in construction. To control the slope's instability, various stabilizing methods were introduced for a new trial section of the canal. Increasing the number of DCM column rows along the canal slope to increase the improvement area was not feasible

due to the budget limitations for this project. Thus, the construction of a stabilized berm at the toe of the canal and the objective to maintain the water at a level of +2.00 m were suggested to limit the creep stress induced by the excavation. Figure 20 shows the stabilized berm with a height of 1 m, a width of 6.1 m, and the same side slope as the excavated canal; the berm was applied in the new trial section of this project. Figure 21a shows the comparison of the factor of safety for the two sections of the canal (with and without remedial measures). The results show that the factor of safety increased from 1.735 (failure case history without a stabilized berm) to 1.887 (new trial section with a stabilized berm). The factor of safety decreased with time due to the effect of undrained creep until a factor of safety of 1.38 was attained after 8 days. Based on the case history, a factor of safety of 1.28 was attained for the unstabilized berm. The berm is useful for increasing the stability

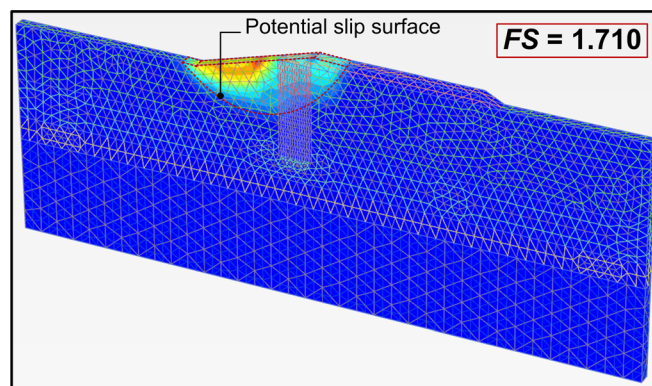


Fig. 16 Slip surface from drainage canal stability analysis immediately after excavation

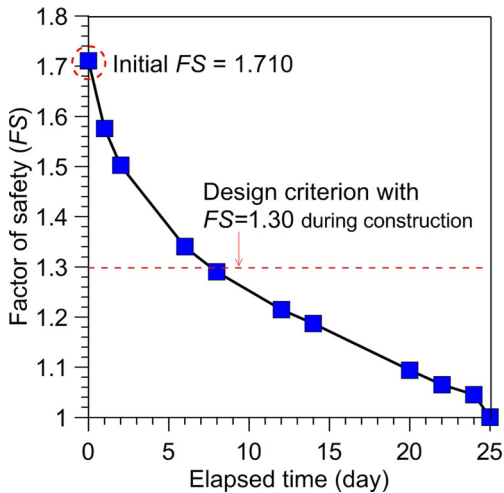


Fig. 17 Factor of safety over time for the case history

to the required value. However, water was released to a level of +2.00 m to counter the lateral movement from creep stress and to prevent instability. The water level of +2.00 m increased the factor of safety from 1.38 to 1.53. The factor of safety was 1.40 after 25 days. Thus, the time period is sufficient to safely complete the roadway construction. The decrease in the average rate of the safety factor

was calculated as 0.00765/day, which is significantly less than the rate in the case history (0.0277/day).

Verification of the adopted solution method was performed by installation of an inclinometer at location I-1, which is the same location in the field case study as shown in Fig. 4. A comparison of the lateral movement profiles with and without a berm and the corresponding water level is shown in Fig. 21b. The lateral movement was substantially less than the lateral movement in the case history. In addition, the rate of lateral movement was significantly reduced from 2 to 0.4 mm/day. Thus, this solution was applied to the entire drainage canal project. The canal has been in service at the proposed water level of +3.00 m for 5 years without any excessive lateral movement by visual observation.

Conclusions

An excavated slope in a soft clay deposit exhibits a viscous creep or undrained creep behavior, in which deformation proceeds at a constant deviator stress. Slope stabilization with DCM columns may be insufficient for preventing failure due to instability. This paper examines the failure of a large drainage canal that is constructed in very soft Bangkok clay. The lateral movements obtained from the field observations continuously increased with time and failed due to the effect of undrained creep. A laboratory investigation including ICU and K_0 CU tests of the undrained creep behavior of soft clay was conducted to assess the creep

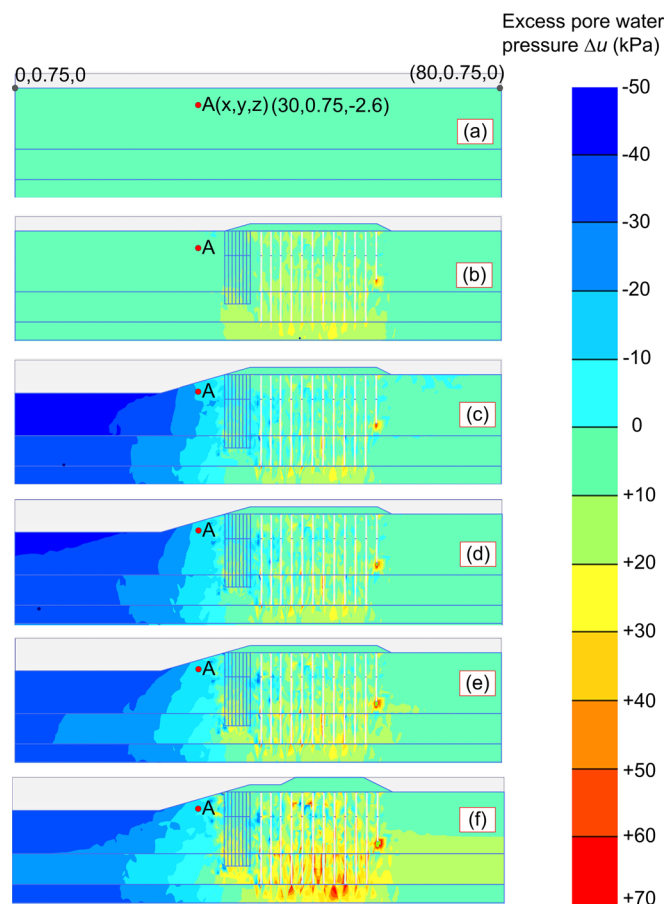


Fig. 18 Excess pore pressure in several stages: *a* initial state, *b* 1.2-m-high roadway construction, *c* at the end of excavation, *d* 2 days, *e* 12 days, and *f* 25 days after the end of excavation (canal failure)

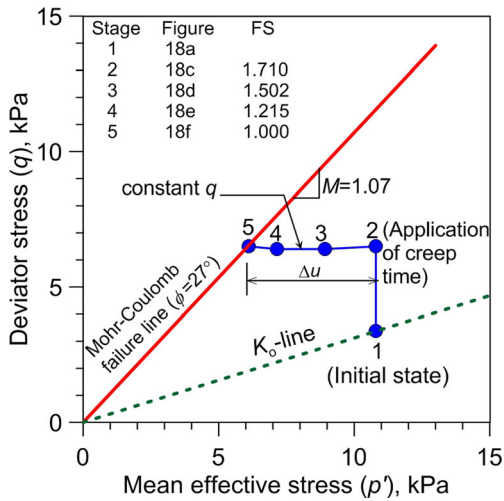


Fig. 19 Stress path of very soft clay at point A under the canal slope

behavior for various constant deviator stresses. A finite element analysis by the PLAXIS 3D software, version 2013, using the SSC model, was performed to confirm the causes of the canal failure. A solution method was introduced to stabilize a new trial section. A comparison of the section with and without remedy was also performed. Based on the results, the following conclusions are formed:

1. The very soft clay located at the excavation base (I-1) exhibits undrained creep behavior beginning with the primary, secondary, and tertiary phases, which caused failure of the canal slope with an average rate of lateral movement of 2 mm/day. The deviator stress in the field is sufficient for generating the shear mobilization of entire phases due to the low strength of the soft clay without soil stabilization by DCM columns. However, this behavior was not observed for very soft clay in zones that were stabilized with DCM columns (I-3) due to the higher strength of the composite ground. Conversely, if soil stabilization is insufficient, very soft clay in this zone will exhibit a creep behavior beginning from the primary to secondary phase and will eventually collapse without clear tertiary phases, such as the very soft clay located at I-2.
2. No creep rupture failure was observed for soft clay specimens at creep stress levels below 50 % of ultimate strength due to the low deviator stress level. This behavior is similar to the field

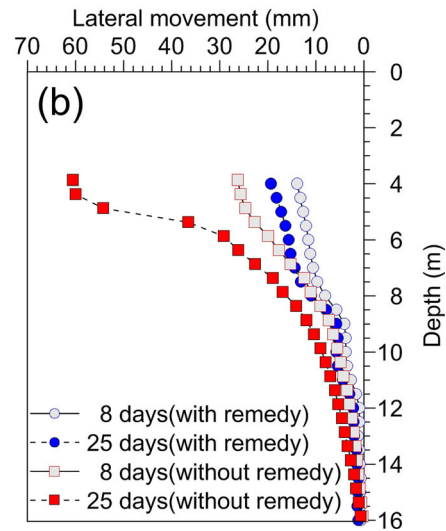
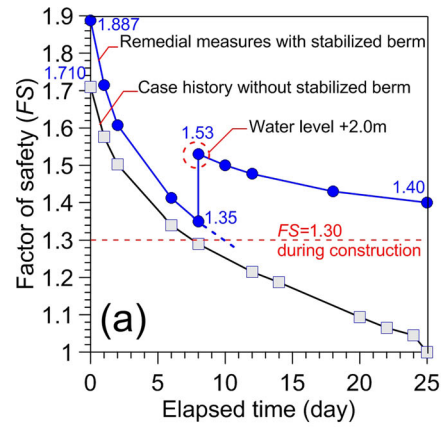


Fig. 21 Comparison of a factors of safety and b lateral movement profiles between the canals with and without remedial measures

observations of the soft clays located in the stabilized zone by the DCM columns (I-3). However, the specimens subjected to a creep stress level range of 70 to 100 % collapsed due to accelerated creep strain rate in the tertiary phases, which caused creep rupture. This process is represented by the maximum lateral movement of soft clay over time without stabilization (I-1). The undrained creep behavior observed from the

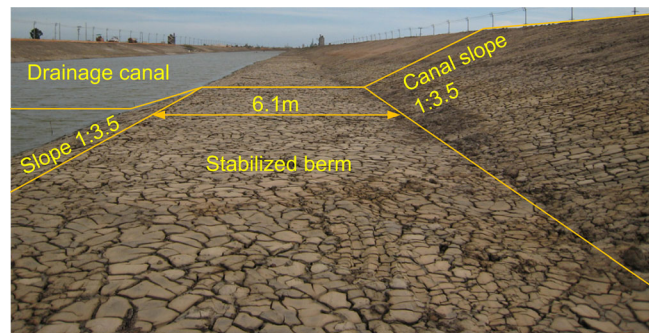


Fig. 20 The stabilized berm for a new trial section of drainage

K_0 CU test represents the field behavior for the creep deformation of very soft clay compared with the results of the ICU test because very soft clay deposits in nature have been subjected to the K_0 condition compared with isotropic compression.

3. Undrained creep reduces the shear strength of very soft clay with time, which causes a decrease in the factor of safety of the excavated slope from its initial value of 1.710 to 1.045 within 24 days after the end of excavation. The average rate of decrease of the factor of safety for the case history after the end of excavation until canal failure was 0.0277/day. The shear strength is reduced because positive excess pore water pressure increases with time.
4. A stabilized berm with a height of 1 m was selected to stabilize a new trial section of the canal to increase the factor of safety. However, 8 days after the end of excavation, the factor of safety tends to be less than the minimum required value of 1.30. Thus, water at the level of +2.0 m was maintained in the canal to counter the creep stress, which causes a higher factor of safety and less lateral movement. The average rate of decrease of the factor of safety was improved to 0.00765/day, which was less than the rate of decrease for the case history without remedial measures. The average rate of lateral movement was also stabilized to 0.4 mm/day. Therefore, the recommended solution works properly to improve both slope stability and lateral movement. The drainage canal has been in service at the proposed water level of +3.00 m for 5 years after the solution was implemented, and no appreciable lateral movement has been observed.

Acknowledgments

The writers gratefully acknowledge the financial support from the Thailand Research Fund (TRF) under TRF Research Scholar Contract No. RSA5580007 and King Mongkut's University of Technology Thonburi under a National Research University (NRU) project.

References

- Anbarasu K, Sengupta A, Gupta S (2010) Mechanism of activation of the Lanta Khola landslide in Sikkim Himalayas. *Landslides* 7(2):135–147
- Arulanandan K, Shen CK, Young RB (1971) Undrained creep behavior of a coastal organic silty clay. *Geotechnique* 21(4):359–375
- ASTM (2012) D4767-02: standard test method for consolidated undrained triaxial compression test for cohesive soils. ASTM International, West Conshohocken
- Atkinson JH, Sallfors G (1991) Experimental determination of soil properties. *Proc 10th ECSMFE* 3:915–956
- Bergado DT, Anderson LR, Miura N, Balasubramaniam AS (1996) Soft ground improvement in lowland and other environments. American Society of Civil Engineers (ASCE) Press, New York
- Bergado DT, Balasubramaniam AS, Long PV (2006) Strength, compressibility and flow parameters for PVD improvement of soft Bangkok clay at SBIA project. *Proceedings of the International Symposium on Geotechnical Aspects of the Second Bangkok International (Suvarnabhumi) Airport in Thailand*. Southeast Asian Geotechnical Society (SEAGS), Bangkok, Thailand, pp. 43–66
- Borges JL, Guerra GT (2014) Cylindrical excavations in clayey soils retained by jet grout walls: numerical analysis and parametric study considering the influence of consolidation. *Comput Geotech* 55:42–56
- Broms BB (1999) Keynote lecture: design of lime, lime/cement and cement columns. *International Conference on Dry Mix Methods: Dry Mix Methods for Deep Soil Stabilization*, Stockholm, Sweden. A.A. Balkema, Rotterdam, Netherlands, pp. 125–153
- Campanella RG, Vaid YP (1974) Triaxial and plane strain creep rupture of an undisturbed clay. *Can Geotech J* 11(1):1–10
- Casagrande A, Wilson S (1951) Effect of rate of loading on strength of clays and shales at constant water content. *Geotechnique* 2(3):251–263
- Chang KT, Ge L, Lin HH (2015) Slope creep behavior: observations and simulations. *Environ Earth Sci* 73(1):275–287
- Desai CS, Sane S, Jenson J (2011) Constitutive modeling including creep-and rate-dependent behavior and testing of glacial tills for prediction of motion of glaciers. *Int J Geomech* 11(6):465–476
- DJM (Deep Jet Mixing) Research Group (1984). *The manual for the dry jet mixing method*. pp. 20–31
- Faruque MO (1986) Modeling of undrained creep of normally consolidated clay. *J Eng Mech* 112(10):1007–1020
- Fatahi B, Le TM, Le MQ, Khabbaz H (2013) Soil creep effects on ground lateral deformation and pore water pressure under embankments. *Geomechanics Geoengeering: Int J* 8(2):107–124
- Holzer TL, Hoeg K, Arulanandan K (1973) Excess pore pressures during undrained clay creep. *Can Geotech J* 10(1):12–24
- Horpibulsuk S, Shibuya S, Fuenkajorn K, Katkan W (2007) Assessment of engineering properties of Bangkok clay. *Can Geotech J* 44(2):173–187
- Horpibulsuk S, Rachan R, Suddeepong A, Chinkulkijniwat A (2011) Strength development in cement admixed Bangkok clay: laboratory and field investigations. *Soils Found* 51(2):239–251
- Horpibulsuk S, Rachan R, Suddeepong A (2012) State of art in strength development of soil-cement columns. *Ground Improvement* 16(4):201–215
- Huang J, Han J (2009) 3D coupled mechanical and hydraulic modeling of a geosynthetic reinforced deep mixed column-supported embankment. *Geotext Geomembr* 27:272–280
- Jamsawang P, Voottipruex P, Boathong P, Mairaing W, Horpibulsuk S (2015) Three-dimensional numerical investigation on lateral movement and factor of safety of slopes stabilized with deep cement mixing column rows. *Eng Geol* 188:159–167
- Jansawang P, Bergado DT, Voottipruex P (2010) Field behavior of stiffened deep cement mixing piles. *Proc Inst Civ Eng Ground Improv* 164(1):33–49
- Kourkoulis R, Gelagoti F, Anastasopoulos I, Gazetas G (2011) Slope stabilizing piles and pile-groups: parametric study and design insights. *J Geotech Geoenviron Eng ASCE* 137(7):663–667
- Kuhn MR, Mitchell JK (1993) New perspectives on soil creep. *J Geotech Eng ASCE* 119(3):507–524
- Larsson S, Malm R, Charbit B, Ansell A (2012) Finite element modelling of laterally loaded lime-cement columns using a damage plasticity model. *Comput Geotech* 44:48–57
- Lefebvre G, LeBoeuf D (1987) Rate effects and cyclic loading of sensitive clays. *J Geotech Geoenviron Eng ASCE* 113(5):467–489
- Leoni M, Karstunen M, Vermeer PA (2008) Anisotropic creep model for soft soils. *Geotechnique* 58(3):215–226
- Lin DG, Liu WT, Lin PC (2006) Numerical analyses of PVD improved ground at reference section of second Bangkok International Airport. *Proceedings of the International Symposium on Geotechnical Aspects of the Second Bangkok International (Suvarnabhumi) Airport in Thailand*. Southeast Asian Geotechnical Society (SEAGS), Bangkok, Thailand, pp. 67–88
- Lorenzo GA, Bergado DT (2004) Fundamental parameters of cement-admixed clay-new approach. *J Geotech Geoenviron Eng ASCE* 130:1042–1050
- Mesri G, Godlewski PM (1977) Time and stress compressibility interrelationship. *J Geotech Eng Div ASCE* 103(5):417–430
- Mitchell JK, Soga K (2005) *Fundamentals of soil behavior*, 3rd edition. Wiley, 577 pp
- Mun B, Kim T, Moon T, Oh J (2012) SCM wall in sand: numerical simulation and design implications. *Eng Geol* 151:15–23
- Redman PG, Poulos HG (1984) Study of two filed cases involving undrained creep. *J Geotech Eng ASCE* 110(9):1307–1321
- Rogers CDF, Glendinning S (1997) Improvement of clay soils in situ using lime piles in the UK. *Eng Geol* 47(3):243–257
- Rosenqvist ITH (1953) Considerations on the sensitivity of Norwegian quick clays. *Geotechnique* 3(5):195–200
- Rukdeecheuai T, Jongpradist P, Wonglert A, Kaewsri T (2009) Influence of soil models on numerical simulation of geotechnical works in Bangkok subsoil. *EIT Res Dev J* 20(3):17–28
- Sexton BG, McCabe BA (2013) Numerical modeling of the improvements to primary and creep settlements offered by granular columns. *Acta Geotech* 8:447–464
- Shen SL, Wang ZF, Horpibulsuk S, Kim YH (2013a) Jet grouting with a newly developed technology: the twin-jet method. *Eng Geol* 152(1):87–95
- Shen SL, Wang ZF, Sun WJ, Wang LB, Horpibulsuk S (2013b) A field trial of horizontal jet grouting using the composite-pipe method in soft deposit of Shanghai. *Tunn Undergr Space Technol* 35:142–151

- Shibuya S, Tmarakar SB, Manakul W (2003) Geotechnical hazards in Bangkok-present and future. *Lowland Technol Int* 5(1):1–13
- Surarak C, Likitlersuang S, Wanatowski D, Balasubramaniam A, Oh E, Guan H (2012) Stiffness and strength parameters for hardening soil model of soft and stiff Bangkok clays. *Soil Foundation* 52(4):682–697
- Taechakumthorn C, Rowe RK (2012) Performance of reinforced embankments on rate-sensitive soils under working conditions considering effect of reinforcement viscosity. *Int J Geomech* 12(4):381–390
- Vekli M, Aytekin M, Ikizler SB, Calik U (2012) Experimental and numerical investigation of slope stabilization by stone columns. *Nat Hazards* 64(1):797–820
- Vermeer PA, Neher HP (1999) A soft soil model that accounts for creep. In: R.B.J. Brinkgreve (ed.), *Proc. Int. Symp. Beyond 2000 in Computational Geotechnics: 10 Years of Plaxis International*: 249–261. A.A. Balkema
- Voottipruex P, Suksawat T, Bergado DT, Jamsawang P (2011a) Numerical simulations and parametric study of SDCM and DCM piles under full scale axial and lateral loads. *Comput Geotech* 38:318–329
- Voottipruex P, Bergado DT, Suksawat T, Jamsawang P, Cheang W (2011b) Behavior and simulation of deep cement mixing (DCM) and stiffened deep cement mixing (SDCM) piles under full scale loading. *Soils Found* 51(2):307–320
- Walker LK (1969) Undrained creep in a sensitive clay. *Geotechnique* 19(4):515–529
- Wang L, Yin Z (2014) Stress dilatancy of natural soft clay under an undrained creep condition. *Int J Geomech*. doi:10.1061/(ASCE)GM.1943-5622.0000271
- Wang L, Zhang G (2014) Centrifuge model test study on pile reinforcement behavior of cohesive soil slopes under earthquake conditions. *Landslides* 11(2):213–223
- Wang D, Bienen B, Nazem M, Tian Y, Zheng J, Pucker T, Randolph MF (2015) Large deformation finite element analyses in geotechnical engineering. *Comput Geotech* 65:104–114
- Yin JH, Zhu JG, Graham J (2002) A new elastic viscoplastic model for time-dependent behaviour of normally and overconsolidated clays: theory and verification. *Can Geotech J* 39(1):157–173
- Yu Y, Shang YQ, Sun HY, Wan EZ (2015) Displacement evolution of a creeping landslide stabilized with piles. *Nat Hazards* 75(2):1959–1976

P. Jamsawang (✉)

Department of Civil Engineering,
King Mongkut's University of Technology North Bangkok,
Bangkok, Thailand
e-mail: pitthaya_kmutnb@hotmail.com

P. Boathong

Department of Civil Technology Education,
King Mongkut's University of Technology Thonburi,
Bangkok, Thailand

W. Mairaing

Department of Civil Engineering,
Kasetsart University,
Bangkok, Thailand

P. Jongpradist

Department of Civil Engineering, Faculty of Engineering,
King Mongkut's University of Technology Thonburi,
Bangkok, Thailand